Geoderma 247–248 (2015) 129–139

Contents lists available at ScienceDirect

Geoderma

journal homepage: www.elsevier.com/locate/geoderma

Carbon dioxide in scree slope deposits: A pathway from atmosphere to pedogenic carbonate

Olivier Hasinger [a], Jorge E. Spangenberg [a], Laure Millière [a], Saskia Bindschedler [b], Guillaume Cailleau [a], Eric P. Verrecchia [a,*]

[a] Institute of Earth Surface Dynamics, University of Lausanne, Geopolis, CH-1015 Lausanne, Switzerland
[b] Institute of Biology, University of Neuchâtel, Rue Emile Argand 11, CH-2000 Neuchâtel, Switzerland

ARTICLE INFO

Article history:
Received 23 July 2014
Received in revised form 18 February 2015
Accepted 22 February 2015
Available online xxxx

Keywords:
Pedogenic carbonate
Carbon dioxide
Stable isotopes
Rock-eval pyrolysis
Soil respiration
Soil organic matter

ABSTRACT

A continuum of carbon, from atmospheric CO_2 to secondary calcium carbonate, has been studied in a soil associated with scree slope deposits in the Jura Mountains of Switzerland. This approach is based on former studies conducted in other environments. This C continuum includes atmospheric CO_2, soil organic matter (SOM), soil CO_2, dissolved inorganic carbon (DIC) in soil solutions, and secondary pedogenic carbonate. Soil parameters (pCO_2, temperature, pH, C_{min} and C_{org} contents), soil solution chemistry, and isotopic compositions of soil CO_2, DIC, carbonate and soil organic matter ($\delta^{13}C_{CO_2}$, $\delta^{13}C_{DIC}$, $\delta^{13}C_{car}$ and $\delta^{13}C_{SOM}$ values) have been monitored at different depths (from 20 to 140 cm) over one year. Results demonstrated that the carbon source in secondary carbonate (mainly needle fiber calcite) is related to the dissolved inorganic carbon, which is strongly dependent on soil respiration. The heterotrophic respiration, rather than the limestone parent material, seems to control the pedogenic carbon cycle. The correlation of $\delta^{13}C_{org}$ values with Rock-Eval HI and OI indices demonstrates that, in a soil associated to scree slope deposits, the main process responsible for ^{13}C-enrichment in SOM is related to bacterial oxidative decarboxylation. Finally, precipitation of secondary calcium carbonate is enhanced by changes in soil pCO_2 associated to the convective movement of air masses induced by temperature gradients (heat pump effect) in the highly porous scree slope deposits. The exportation of soil C-leachates from systems such as the one studied in this paper could partially explain the "gap in the European carbon budget" reported by recent studies.

1. Introduction

Soil carbon is the fourth largest pool of C, when including pedogenic carbonates sequestered in sediments and rocks (Retallack, 2007; Lal, 2009). The soil C pool has received increasing attention, since the sustainability of the ocean C sink is being questioned (Le Quéré et al., 2007). In terrestrial environments, C sequestration is almost entirely attributed to soil and plant organic C storage, while the contribution of soil mineral C is generally neglected (Sanderman, 2012), as well as the combined action of carbonate dissolution and the global water cycle (Liu et al., 2010).

Although CO_2 transfers at the soil–atmosphere interface have been thoroughly studied (Bond-Lamberty and Thomson, 2010), the CO_2 consumption and release through mineral weathering (Szramek et al., 2007; Jin et al., 2009; Liu et al., 2010), as well as the continuum between soil organic matter (SOM) – soil CO_2 – dissolved inorganic carbon (DIC) remains poorly documented. Recent studies have emphasized the importance of the relationships between C dynamics in the soil solution (gas dissolution and weathering) and the soil carbonate formation, as they can play an important role in the sequestration of atmospheric CO_2 (Manning, 2008; Ryskov et al., 2008; Renforth et al., 2009; Jin et al., 2009). The link between SOM, soil CO_2, and precipitation of secondary carbonates has been described in arid and semi-arid environments for a long time (Cerling, 1984; Cerling et al., 1991; Nordt et al., 1996), but the interactions between those compartments have been less studied in temperate ecosystems. The assessment of the relationships between stable isotopes and soil physicochemical conditions constitutes a conventional tool in the study of processes involved in the terrestrial carbon cycle (Clark and Fritz, 1997; Ehleringer et al., 2000) and the dynamics of soil organic (Wynn et al., 2006; Boström et al., 2007) and inorganic carbon (Aravena et al., 1992; Clark and Fritz, 1997; Jin et al., 2009).

Stable C isotope compositions differ between the various soil compartments. Because of the higher vibrational frequency of the light ^{12}C isotope compared to the heavy ^{13}C isotope, fractionations occur during physicochemical reactions. For example, ^{12}C isotope is favored by the biological system during photosynthesis in order to optimize the energy

* Corresponding author.
E-mail address: eric.verrecchia@unil.ch (E.P. Verrecchia).

http://dx.doi.org/10.1016/j.geoderma.2015.02.012
0016-7061/

expense (Urey, 1947; Park and Epstein, 1960). The stable C isotope signature of SOM, soil CO_2, DIC, and pedogenic and lithogenic carbonates differ predictably (Cerling et al., 1991; Clark and Fritz, 1997).

The C content of soil gas in vadose environments is mainly attributed to the $CO_{2(g)}$ source (Cerling, 1984). $CO_{2(g)}$ concentrations in soil pores at any given depth are driven by two main parameters: i) the intensity of biological activity; ii) the diffusion processes that control the transfer of gas mass, inducing the mixing of atmospheric CO_2 and soil-respired CO_2 in the topsoil and in the lower layers. Previous studies showed that $\delta^{13}C$ values of soil CO_2 are higher in the topsoil, due to an enhanced diffusion of $^{12}CO_2$ at the soil–atmosphere interface (Cerling and Wang, 1996). In addition, in most of soils, C isotope composition of soil $CO_{2(g)}$ from the deeper horizons tend to be similar to the $\delta^{13}C$ values of SOM. Furthermore, when rain infiltrates into the soil, it equilibrates with the soil CO_2, leading to the diffusion of $CO_{2(g)}$ into the soil solution, a process contributing to the isotopic composition of the DIC species: $CO_{2(aq)}$, H_2CO_3, HCO_3^-, and CO_3^{2-}.

Concentrations of the various carbonate species depend on pH and temperature of the soil solution (Clark and Fritz, 1997). In an open system, the soil solution is only slightly influenced by the dissolution of lithogenic carbonates because soil $CO_{2(g)}$ constitutes an infinitely larger reservoir of carbon (Nordt et al., 1996). The resulting precipitation of pedogenic carbonate from the soil solution ($HCO_3^-{}_{(aq)}$) is thus normally in isotopic equilibrium with the soil $CO_{2(g)}$ (in terms of concentrations and C isotope composition) at a given soil depth (e.g., Cerling et al., 1989; Cerling and Wang, 1996; Deutz et al., 2001).

In this study, in order to document C dynamics in the SOM – soil CO_2 – DIC continuum, a stable C isotope approach has been chosen. This approach is based on soil parameters (pCO_2, temperature, pH, C_{min} C_{org} content), stable isotope compositions of soil organic and inorganic carbon species ($\delta^{13}C_{SOM}$, $\delta^{13}C_{DIC}$ and $\delta^{13}C_{car}$ values), as well as a monitored acquisition of field data. The aim of this study focuses on the following points. i) The continuum between CO_2 and pedogenic carbonate (needle fiber calcite — NFC and late calcitic cements — LCC; Millière et al., 2011a) is investigated through the leading processes involved in soil carbon transfers (from CO_2 to DIC) in a temperate carbonate soil system. The chosen site is situated in the Swiss Jura Mountains and is associated with scree slope deposits. ii) The second aim is to assess the origin of carbon in both LCC and NFC end-members. iii) In addition, interactions between soil CO_2 and DIC will be documented for a specific soil system, i.e. a carbonate soil developed in coarse cryoclasts. iv) Finally, the ^{13}C enrichment of SOM with increasing depth will be discussed. The results of this study show that pedogenic carbonate found in soils from the Swiss Jura Mountains mainly originates from atmospheric CO_2 rather than redistribution from the carbonate bedrock through dissolution and reprecipitation processes.

2. Field site description

2.1. Geographical settings

The study area is located in the central part of the Swiss Jura Mountains, approximately 15 km north of Neuchâtel in western Switzerland (Fig. 1). Cretaceous and Jurassic limestones, in a succession of anticlines and synclines, compose the predominant bedrock of the region. A reference soil in Villiers (47°04′N, 6°59′E, 769 m asl) has been chosen for the monitoring of the various soil compartments (SOM, soil gas, and soil solution) due to its exceptional abundance of secondary carbonate in the deep horizons (Fig. 2; Millière et al., 2011a). The studied soil is situated at the foot slope of an anticline, which is affected by two important overthrusts (Burkhard and Sommaruga, 1998). Kimmeridgian limestone forms the upper part of the slope, whereas its lower part corresponds to glacial tills covering a Portlandian micritic limestone. Scree slope deposits at the foot slope contain frost-shattered fragments of both Jurassic limestones, cryoclasts being covered by the studied soil (Fig. 2), situated at approximately 20 m laterally to a small (<2 m high) quarry front.

The climate in the study area, as in all areas north of the Alps, is influenced by both oceanic (West European) and continental (East European) conditions. The oceanic climate is most prominent in the region of the Swiss Jura where the reference soil of Villiers is situated. The region is exposed to westerly winds bringing warm and wet air masses, with a rainfall often exceeding 1400 mm/year. The climate record in this region reports a mean annual rainfall of 1200 mm, and a mean annual temperature of 6 °C (January $T = -1$ °C; July $T = 18$ °C; MétéoSuisse, 2008). The soil is covered by snow during winter and the beginning of spring. The study area is covered by C_3 forest vegetation, dominated by beech trees (*Fagus sylvatica*) and subordinate species such as fir trees (*Abies alba*), and spruce trees (*Picea abies*). The underbrush is poor due to low luminosity caused by the dense foliage of beech trees.

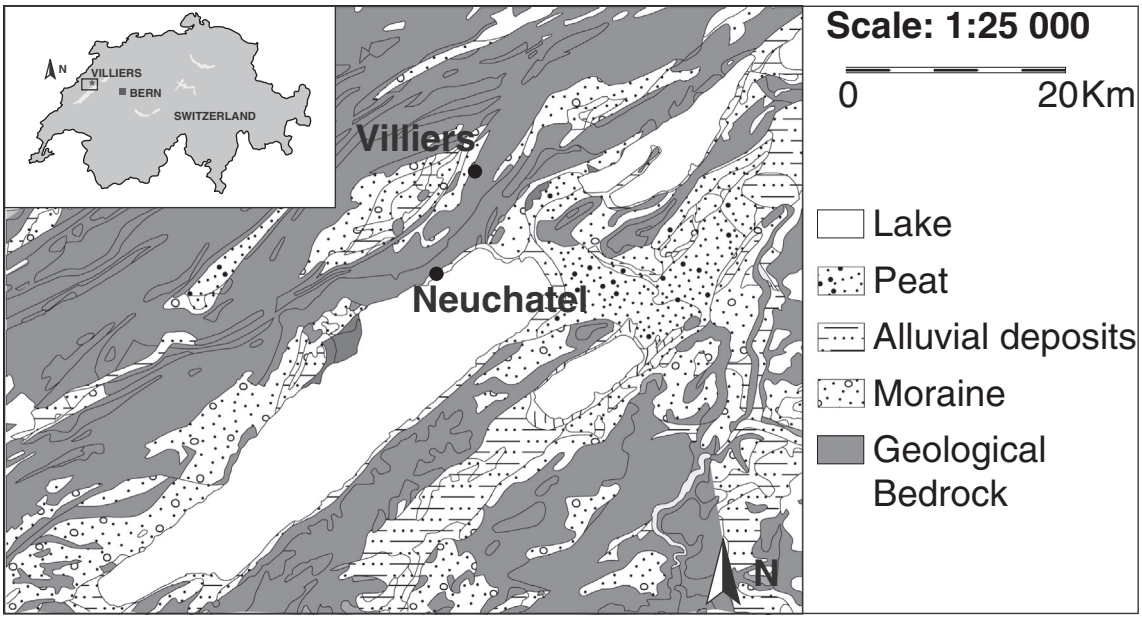

Fig. 1. Location of the study area in Switzerland and geological map of the eastern part of the canton of Neuchâtel.

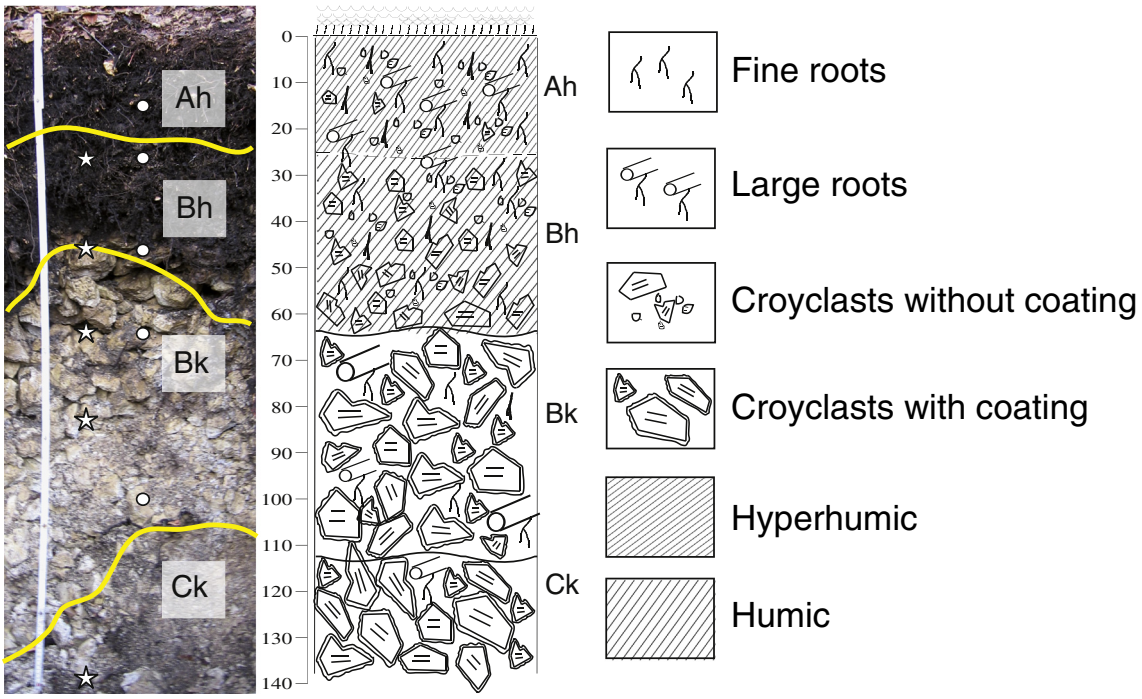

Fig. 2. Soil profile, Villiers (canton of Neuchâtel, Switzerland). The soil is divided into two main layers, each being divided into two sub-layers: 1) Ah and Bh horizons are microporous and enriched in organic matter; 2) Bk and Ck horizons are composed of calcareous scree deposits enriched in secondary pedogenic carbonate in pores between cryoclasts (mainly as needle fiber calcite — NFC and late calcitic cements — LCC). Pores in Bk and Ck horizons are centimetric to pluri-centrimetric in size. The stars refer to the soil CO_2 sampling depths and the circles to the soil water sampling depths.

2.2. Soil description

The calcareous soil at Villiers (Fig. 2) developed during the Holocene under a temperate climate, after the last Alpine glaciation (Würm; Dalla Piazza, 1996). It can be defined as a hypocalcic Calcisol (hyperhumic skeletic) (IUSS, 2006). The uppermost soil horizons, Ah and Bh, contain a large amount of well-preserved organic matter with an organic C (C_{org}) content of 21.6 and 9.3 wt.%, respectively. They lie on two mineral horizons (Bk and Ck horizons) composed of 98% lithogenic carbonate pebbles and secondary pedogenic carbonate including NFC and LCC (>10% $CaCO_3$ in the fine earth). These secondary carbonate features are observed between 65 and 140 cm in depth (Fig. 2). Millimetric pores dominate the upper soil from the surface to 70 cm in depth, whereas centimetric pores and a low content in organic matter (2.4 wt.%) characterize the deep mineral horizons. There is a high porosity between cryoclasts in Bk and Ck horizons, leading to intense water drainage of the entire soil. In addition, the packing of large amounts of centimetric limestone pebbles in Bk and Ck horizons induces a highly interconnected macroporosity (estimated between 20 and 30% according to visual charts), facilitating gas mass transfers within the soil profile in all directions. Finally, the boundary between the Bh and Bk horizons is sharp and undulated. It has to be noted that Ah and Bh horizons develop in a colluvium-enriched deposit, whereas scree slope deposits constitute the Bk and Ck parent materials.

3. Methods

3.1. Sample collection

3.1.1. Bulk soil samples

These samples were collected from a 1.4 m deep soil profile based on a systematic sampling strategy. The excavation for the soil profile was 1.20 m in width and length, and 1.40 m in depth. Soil samples were collected according to soil horizons. The bulk soil was sampled at 10 cm intervals inside the two uppermost horizons (between the surface and 80 cm in depth). For the lower part of the profile (between 80 and 140 cm), the samples were collected only every 20 cm, due to the high homogeneity of the deep soil layers (Table 1). For soil solution and gas sampling, an effort was made to get material as close as possible to the sampled soils. This was not always achievable because of the physical constraints due to the nature of the coarse parent material.

3.1.2. Soil CO_2

Five soil gas tubes were installed vertically in the soil at 27, 49, 67, 81 and 143 cm depth (Fig. 2, star symbols) from the surface in holes previously obtained with a digging bar. The sampling device consisted of 1 mm interior diameter brass tubes equipped with flasks at each end. At the basal part, the flasks were sealed to the tube and turned upside down to avoid obstruction by soil particles, and on the other end, the sealed flasks were equipped with a silicone septum-cap for sampling of soil gas with 10 mL gastight syringes (Sample-LoK™ A-2 gas type made by VICI®). After each gas sampling, silicone septum-caps were replaced. Aluminum tubes of large diameter (12 mm in diameter) were

Table 1
Organic and inorganic C (C_{org} and C_{min}, respectively) content, hydrogen index (HI) and oxygen index (OI), bulk soil pH_{H2O} and $\delta^{13}C$ (in ‰ VPDB) of the soil organic matter (SOM) in the reference profile from Villiers scree slope deposit.

Depth (cm)	pH_{H_2O}	C_{org} (wt.%)	C_{min} (wt.%)	HI (mg HC/g C_{org})	OI (mg CO_2/g C_{org})	$\delta^{13}C_{SOM}$ (‰ VPDB)
10	7.7	21.38	1.58	186	183	−26.9
20	7.8	19.05	3.08	174	190	−26.2
30	8	11.30	6.09	154	203	−25.4
40	8.1	8.19	6.91	144	207	−25.2
50	8.2	6.64	7.28	136	219	−25.1
60	8.3	5.70	7.73	126	240	−25.0
70	8.3	4.13	8.60	126	291	−25.0
80	8.3	2.54	9.54	115	341	−25.0
100	8.4	2.29	10.13	109	348	−25.0
120	8.4	1.91	10.26	85	393	−25.0
140	8.5	1.83	10.64	84	377	−25.3

used as guides for the installation of the sampling tubes. The installed device has rested for 6 months for stabilization before any sampling. The sampling device (syringes and tubes) was maintained open for a minute to avoid any isotopic fractionation between soil gas and gas sample in the syringe. Gas samples were transferred into gastight bags (Cali-5-bond™ by GRACE®) for further laboratory analysis.

3.1.3. Soil solution

PTFE/Quartz lysimeters (tension soil water collector, 21 mm in diameter, 95 mm in length, and with a 2 μm pore size) were installed in a similar way as the gas tubes. They were inserted in the soil at the corresponding depths of the soil CO_2 sampling device (15, 27, 49, 67, 100 and 157 cm; Fig. 2, circle symbols). The porous cup-type lysimeters ensured that soil solution samples were in equilibrium with soil physicochemical conditions at a given depth. The sampling device could hold a vacuum of −0.8 Bar for adequate pumping of the soil solution (Jin et al., 2009). After the installation, lysimeters stayed in the ground for six months (September 2007 to March 2008) before the first sample collection. This stabilization time was necessary to minimize the disturbance to the system during installation of the sampling device. The real range of the sampling depth for the soil water (collected by the tension lysimeters) is at least 10 cm, considering the cup length and the zone of influence of the capillary forces. It was not possible to ensure an optimal hydraulic conductivity between lysimeters and soil matrix for soil solution sampling in the mineral horizons with significant macroporosity (Bk and Ck horizons). In these horizons, the soil water samples were collected from polypropylene trays (340 cm^2) buried at depths of 100 cm and 157 cm. The trays were inserted horizontally in a dug-out soil profile refilled with excavated sediment, respecting the horizon succession. Sampling started only 6 months later to allow soil stabilization. Water from the small brook situated at the foot of the anticline, about fifty meters below the study site, has been sampled at the same time as the soil solution, approximately monthly (Table 2), in order to evaluate the order of magnitude of outputs from the "soil + surficial deposits + geological layers" system. Soil water samples were filtered in the field through 0.45 μm Exapure™ nylon membrane filters into pre-cleaned glass bottles. Several aliquots for each type of analysis were transferred into 2 mL crimped glass vials (SHG P628/650 by Chromacol Ltd). For cation analyses, one aliquot of each sample was acidified to pH < 2 with high-purity nitric acid (SupraPure®) and stored frozen. For DIC concentration and C isotopic composition analyses, inhibition of any biological activity in samples was made by adding 30 μL of a 0.1 M sodium azide solution per mL of sample. In addition, crimped vials were hermetically sealed to avoid any exchange with the atmosphere during storage, in order to avoid any alteration of the DIC concentration and its C isotopic composition.

3.2. Analyses of bulk soil

The bulk soil samples were dried at ambient air temperature, sieved to 2 mm, and preserved at room temperature for laboratory analysis. Soil C_{org} and carbonate contents were measured using Rock-Eval 6™ pyrolysis (Disnar et al., 2003; Sebag et al., 2006) with approximately 70 mg of bulk soil. The sample was weighed and pyrolyzed under a gradual increase of temperatures. This step was followed by the complete oxidation of the residual sample (Espitalié et al., 1985a,b; Lafargue et al., 1998). A flame ionization detector (FID) measured the amount of hydrocarbon released during pyrolysis, while CO_2 and CO were detected by infrared absorbance during both steps. The pyrolysis starts isothermally at 300 °C for three minutes. A S1 peak gave the amount of hydrocarbons released during this isothermal phase. Then, the sample was heated to 650 °C. A S2 peak provided the content of hydrocarbons produced between 300 and 650 °C. An oxidation step started isothermally at 400 °C and lasted for another three minutes, resulting in a S3 spectrum that gives the curve of CO_2 released during pyrolysis. Finally, the sample was heated up to 850 °C to determine the amount of inorganic carbon contained in the sample. Soil organic carbon (C_{org}) and inorganic carbon (C_{min}) contents were expressed in percentage by weight. A hydrogen index ($HI = (S2_{area} \times 100) / C_{org}$) in mg of hydrocarbons per g of C_{org} and an oxygen index ($OI = S3_{area} \times 100 / C_{org}$) in

Table 2
Soil water composition and calculated saturation index of calcite from Villiers scree slope deposit. NA (not available).

Date	Depth (cm)	pH	Temp (°C)	DIC (mmol/l)	$\delta^{13}C_{DIC}$ (‰ VPDB)	Ca^{2+} (μmol/l)	Mg^{2+} (μmol/l)	$SI_{calcite}$
13.03.08	49	7.4	3.45	1.26	−11.7	1061	34	−0.79
13.03.08	67	7.8	3.6	2.74	−11.0	1381	40	0.04
13.03.08	Output[a]	7.7	3.75	6.20	−13.9	1992	268	0.4
19.03.08	27	NA	3.75	1.04	−11.8	NA	NA	NA
19.03.08	49	8.21	3.9	1.73	−11.4	1116	38	0.17
19.03.08	67	8.13	3.8	2.19	−11.6	1354	36	0.26
19.03.08	Output[a]	7.73	3.8	8.02	−13.6	1876	258	0.51
01.04.08	49	7.93	4.4	2.10	−11.3	1186	116	0.01
01.04.08	67	8.17	4.1	2.18	−11.6	1319	36	0.3
01.04.08	Output[a]	7.76	3.9	3.40	−12.4	1902	358	0.2
11.04.08	27	NA	5.3	1.20	−9.8	NA	NA	NA
11.04.08	49	8.17	4.9	1.81	−10.4	1052	33	0.14
11.04.08	67	8.3	4.5	2.09	−10.6	1302	40	0.41
11.04.08	Output[a]	7.65	4.0	3.41	−12.4	1738	251	0.06
23.04.08	15	7.99	6.1	2.95	−11.3	1610	65	0.35
23.04.08	27	NA	6.1	0.93	−11.6	NA	NA	NA
23.04.08	49	7.98	5.45	2.10	−11.2	1149	34	0.06
23.04.08	67	8.04	4.8	2.43	−11.1	1326	33	0.23
23.04.08	Output[a]	8.11	4.05	3.22	−12.4	1607	235	0.46
28.05.08	15	8.27	10.2	1.92	−12.8	1802	65	0.55
28.05.08	49	8.33	9	1.86	−12.5	1476	40	0.5
28.05.08	67	NA	7.85	2.81	−11.9	NA	NA	NA
28.05.08	Output[a]	8.26	6.35	3.50	−12.9	1734	244	0.75
12.06.08	15	8.29	10.55	2.15	−12.0	1819	62	0.63
12.06.08	27	NA	10.55	2.90	−10.9	NA	NA	NA
12.06.08	49	8.37	10.15	2.40	−11.2	1920	48	0.76
12.06.08	67	NA	9.3	2.66	−12.0	NA	NA	NA
12.06.08	Output[a]	8.21	7.65	3.84	−13.5	1880	249	0.75
20.09.08	100	7.7	11.45	2.00	−14.8	1910	76	0.05
20.09.08	157	7.43	11.2	2.06	−16.1	2825	200	−0.06

[a] Samples collected in a small brook situated at the foot of the anticline about fifty meters below the study site (reference points).

mg of CO_2 per g of C_{org} have been calculated to describe the quality and the degradation degree of the SOM. Measurements were calibrated using two standards (IFP 160000 and VP143h). Errors relative to standard IFP 160000 were approximately 0.77, 0.25, and 1.5% for TOC, HI and OI indices, respectively.

Crushed and homogenized soil samples were decarbonated with 10% HCl and the C isotope composition of the SOM ($\delta^{13}C_{SOM}$ values) was determined by elemental analysis–isotope ratio mass spectrometry (EA–IRMS) with a Carlo Erba 1108 connected to a Thermo Fisher Delta V IRMS (Bremen, Germany) at the University of Lausanne. Carbon isotope compositions are reported in the delta (δ) notation as the per mil (‰) deviation relative to the Vienna Pee Dee Belemnite limestone (VPDB) standard, where $\delta = (R_{sample} - R_{standard}) / R_{standard} \times 1000$ with $R = {}^{13}C/{}^{12}C$. The standard error was ±0.1‰ VPDB.

Soil physicochemical parameters were measured along the profile. Soil pH was obtained using a 827 pH-meter from Metrohm® AG, calibrated with pH 7 and pH 9 technical buffers and a 1:2.5 ratio for soil:H_2O. The estimated uncertainty is ±0.05 pH units. The soil temperature was measured in the field with five Grant Squirell Monitoring probes with an uncertainty of ±0.05 °C.

3.3. Analysis of soil gas

Soil pCO_2 was measured in the field with a portable CO_2 infrared analyzer (ATX 620 Multigas Analyser), calibrated with four CO_2 standards ranging from 0 to 50,000 ppm. The standard error, estimated at ±67 ppm, was determined by a regression function obtained from repeated measurements of CO_2 standards of known concentrations. The C isotopic composition of the soil CO_2 ($\delta^{13}C_{CO_2}$ values) was measured using a continuous flow gas chromatograph–combustion–isotope ratio mass spectrometry system (GC connected to a Thermo Fisher Delta Plus XL IRMS) at the University of Neuchâtel with a 250 µl loop and a *Poraplot Q* GC column. The standard error is ±0.14‰ VPDB.

3.4. Analyses of soil water

The soil solutions were sampled and analyzed over a period of six months. DIC concentration and carbon isotopic composition ($\delta^{13}C_{DIC}$ values) were determined using 2 mL aliquots of soil water samples that were degassed by acidifying the sample with pure H_3PO_4. The released CO_2 was analyzed for its isotopic composition using a Thermo Fisher GasBench II connected to a Delta Plus XL IRMS at the University of Lausanne. The DIC concentration was determined after the method described by Assayag et al. (2006). Laboratory standards were calibrated relative to international standards. The analytical reproducibility estimated from replicate analyses of the laboratory standard Carrara marble was better than ±0.05‰ for $\delta^{13}C$.

The two major cations (Ca^{2+} and Mg^{2+}) involved in carbonate precipitations were analyzed by ion chromatography (IC; Dionex®). Reproducibility and accuracy (reported as mean standard deviation) were better than ±3% and the detection limit was 0.1 mg/L. Finally the calculation of element speciation and mineral saturation indices were performed by the geochemical modeling code PHREEQC-2 (Parkhurst and Appelo, 1999). The saturation index of calcite ($SI_{calcite}$ = log [IAP / Ksp], where IAP = ion activity product and Ksp = constant of the solubility product of calcite at room temperature) has been calculated using the following parameters: pH, concentrations of Ca^{2+}, Mg^{2+}, DIC, and temperature.

4. Results

4.1. Physicochemical parameters

4.1.1. Seasonal variations of soil CO_2 concentrations

Soil CO_2 concentrations vary between 520 and 5390 ppm (Fig. 3). In contrast to the common vertical distribution of CO_2 in soil profiles, the uppermost horizons (from surface to 70 cm; Ah and Bh horizons) are clearly distinguishable throughout the year. CO_2 concentrations decrease systematically according to the depth, contrary to what can be found in the literature (Fierer et al., 2005; Kutsch et al., 2009). In summer, this phenomenon is even more pronounced, with a maximal difference of CO_2 concentrations equal to 3130 ppm between 27 cm and 143 cm deep during July. In winter, the soil CO_2 concentrations are very low at all depths, but remain always higher than the atmospheric pCO_2. They do not exceed 2000 ppm and vary around a mean value of 1400 ppm (Fig. 3). From November to April, the difference in terms of CO_2 concentrations between the uppermost and the mineral horizons is no longer significant.

4.1.2. Seasonal variations in the soil temperatures

The evolution of the soil temperatures, according to time and depth, is shown in Fig. 3. The vertical profiles of soil temperatures are inverted twice during the year (mid-March and mid-September). According to this observation, the annual variation of soil temperatures can be divided into two main periods: a cold period from November 2007 to April 2008, and a warm period from May 2008 to September 2008. There is an increasing positive difference between the ambient (surficial atmosphere) and soil temperatures during the transition from the coldest to warmest periods. The maximum difference of temperature between top and bottom of the soil profile occurs during July. This soil temperature gradient, associated with the ambient atmospheric temperature, results in transfers of gas masses from the soil to the atmosphere due to convection of air masses. This is corroborated by the pCO_2 distribution in the soil profile throughout the year.

In terms of temperature, the soil is a buffered system compared to the surficial atmosphere, which fluctuates largely at the short-term scale (Fig. 3; Millière et al., 2011a). At a depth of 24 cm, temperature varies between a maximum of 14.2 °C ± 0.05 °C in July and a minimum of 1.2 °C ± 0.05 °C in February. The mean annual soil temperature in the mineral horizons, characterized by an important macroporosity (from 66 to 130 cm), is 7.3 °C ± 3.3 °C (n = 15).

4.1.3. Vertical profile of pH, C_{org} and C_{min} contents, and $\delta^{13}C_{SOM}$

The pH values of the bulk soil increase with depth from 7.7 for the 0–10 cm interval to 8.5 for the deepest sampling interval (120–140 cm; Table 1). Vertical profiles of pH and C_{min} show similar distributions, whereas C_{org} values display an opposite trend. The pH values are obviously related to the acidifying effect of the organic matter in the uppermost horizons. The increasing carbonate content buffers bulk soil pH in the mineral horizons (Table 1).

C_{org} and C_{min} contents, as well as OI/HI values of SOM, are given in Table 1. The C_{org} content in bulk soil samples underlines a clear distinction between the uppermost horizons enriched in organic matter (from surface to ~70 cm; Ah and Bh horizons) and the deep mineral horizons characterized by a coarse skeleton with a low C_{org} content (from ~70 cm to ~140 cm; Bk and Ck horizons). OI values increase with depth from 183 to 377 mg CO_2/g C_{org}. HI values decrease rapidly in the first 60 cm, from 186 to 126 mg HC/g C_{org} (Fig. 4), and then more gradually in the deepest eighty centimeters (from 126 to 84 mg HC/g C_{org}; Fig. 4). OI values show an opposite trend compared to HI. In the top 60 cm, OI values increase from 183 to 240 mg CO_2/g C_{org} (Fig. 4), rising up to 377 mg CO_2/g C_{org} in the deepest eighty centimeters (Fig. 4). The C isotopic composition of SOM varies between −26.9 and −25.0‰ with depth (Table 1; Fig. 5). In addition, there is a marked ^{13}C enrichment with increasing depth. Finally, there is a clear relationship between HI and OI indices and $\delta^{13}C_{SOM}$ values (Fig. 4 and Table 1).

4.1.4. Seasonal variations of the soil solution and its chemical characterization

$SI_{calcite}$ values of the soil solution are given in Table 2. The increasing $SI_{calcite}$ values range from near 0 to 0.8 over the April and June sampling

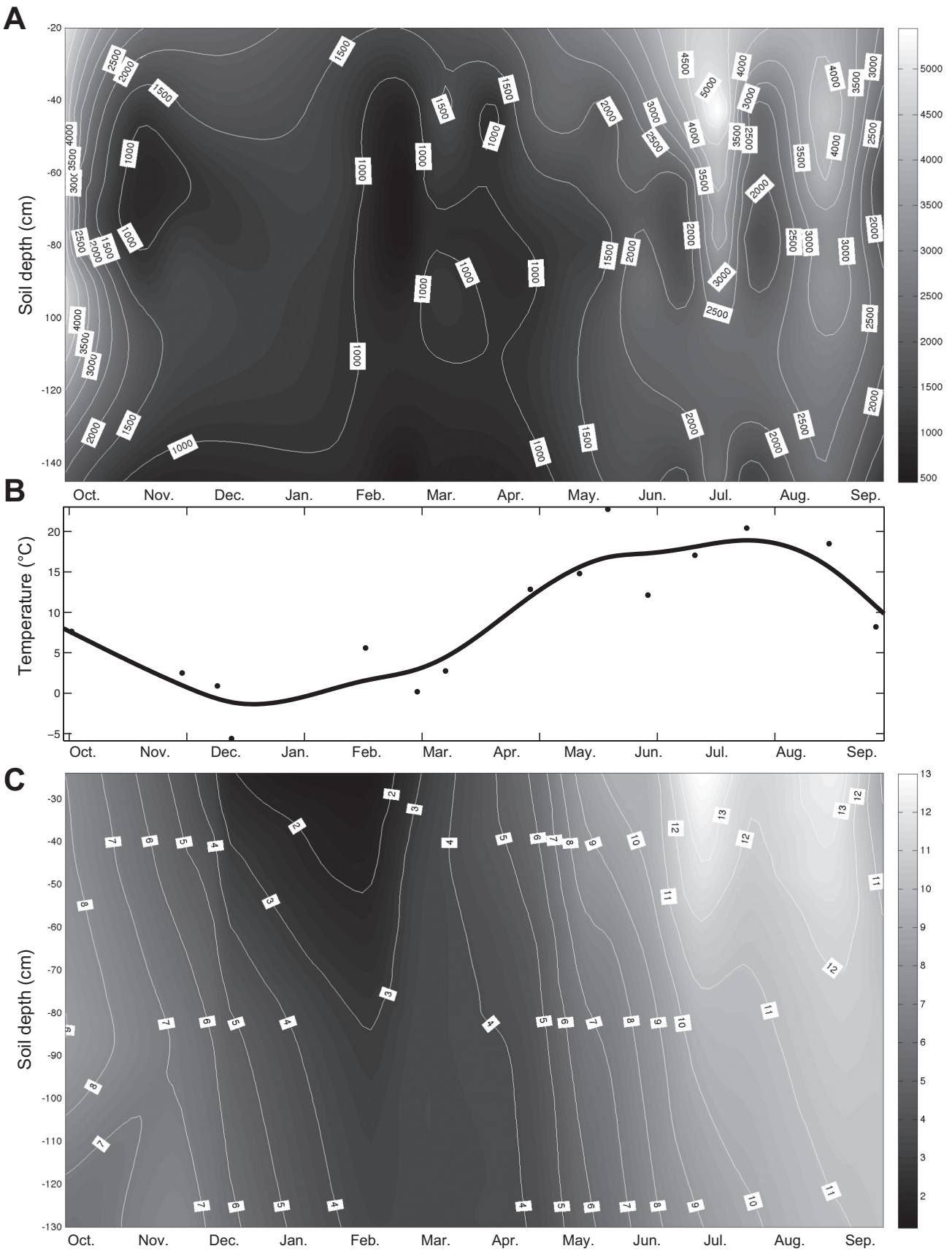

Fig. 3. (A) Seasonal evolution of soil CO_2 concentrations from October 2007 to September 2008 in function of depth expressed with isovalue curves. (B) Seasonal evolution of the atmospheric temperature (at 1.5 m from the ground) over a one-year period of monitoring. (C) Seasonal evolution of the soil temperature at various depths over a one-year period of monitoring from October 2007 to September 2008, expressed with isovalue curves.

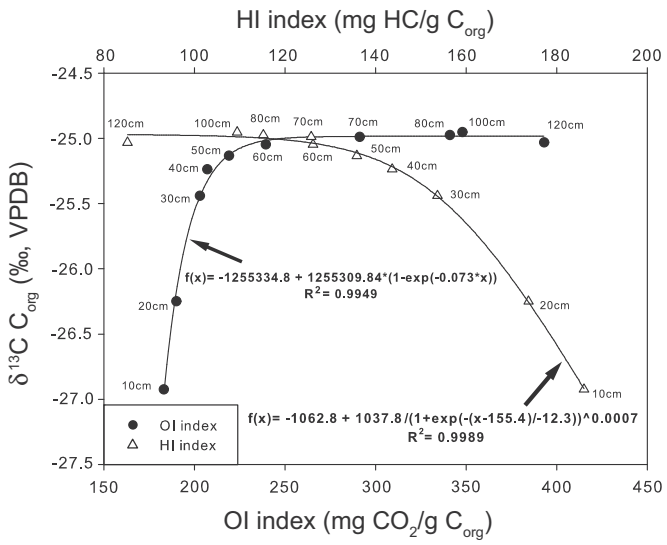

Fig. 4. $\delta^{13}C_{SOM}$ values vs the Rock-Eval OI and HI values. A nonlinear relationship exists between the values as modeled by the two given exponential equations with $r^2 > 0.99$. Sample points are perfectly positioned along the curve in function of depth.

periods, and point to an increasing potential for calcium carbonate precipitation in summer.

4.2. C isotope composition of soil CO_2

The $\delta^{13}C_{CO_2}$ values measured along the soil profile between 27 cm and 143 cm deep are listed in Table 3. During summer, the $\delta^{13}C_{CO_2}$ values show an unusual distribution compared to the common model by Cerling et al. (1991). A trend towards higher $\delta^{13}C_{CO_2}$ values with increasing depth is observed in June and July (Fig. 5). The $\delta^{13}C_{CO_2}$ values vary much less with depth during the warm period between early spring and late fall. A process that could explain this trend is discussed below (see Section 5.1).

Differences in C isotope composition of soil CO_2 between the uppermost (organic-rich) and mineral horizons are not significant in early spring and late fall profiles, but clearly different for both summer profiles (June and July). These differences (between 27 cm and 143 cm) are −0.48‰ and −0.36‰ VPDB for March and November, respectively, and +2.3‰ and +1.7‰ for June and July (Fig. 5).

The large differences in $\delta^{13}C_{CO_2}$ values between the top and deepest horizons during the warm period reflect a significant ^{13}C-enrichment of CO_2 in the mineral horizons, which are characterized by a coarse skeleton and a high macroporosity. This ^{13}C enrichment in the mineral horizons does not follow the commonly observed variation of the C isotopic composition of soil CO_2 with depth (Cerling and Wang, 1996; Liu et al., 2006; Kutsch et al., 2009).

4.3. C isotope composition of DIC in soil solution

The $\delta^{13}C_{DIC}$ values vary between −12.8‰ and −9.8 ± 0.06‰ in the uppermost horizons over the entire 6-month period of sampling (Table 2). For the mineral horizons, the $\delta^{13}C_{DIC}$ values are −14.8 ± 0.4‰ and −16.1 ± 0.08‰ at a depth of 100 cm and 157 cm, respectively (Fig. 6 and Table 2). $\delta^{13}C_{DIC}$ values of the reference-sampling site (a small brook situated at the foot of the anticline, fifty meters below the study site) vary between −13.9‰ and −13.5‰ from March to June (Table 2). These $\delta^{13}C_{DIC}$ values measured in the brook were systematically and significantly more negative than those of the soil solution (Fig. 6 and Table 2).

The $\delta^{13}C_{DIC}$ values showed that the soil solution was in equilibrium with the soil CO_2 at a given depth. The values fall within the theoretical equilibrium interval (between the two dashed lines, Fig. 6) when considering the soil as an open system. This implies that the CO_2 from soil pores was in chemical equilibrium with the DIC of the soil solution, at the measured pH and temperature (Fig. 6).

5. Discussion

5.1. Lateral and vertical diffusive fractionation in scree slope soils

The average C-isotopic fractionation values between the SOM and the soil CO_2 ($\Delta_{org\text{-}CO_2} = \delta^{13}C_{SOM} - \delta^{13}C_{CO_2}$) shows unexpected variations along the soil profile (Fig. 7). The $\Delta_{SOM\text{-}CO_2}$ values vary from 3.9 to 3.2‰ between the Ah and Bh–Bk horizons, and then the trend is reversed and rises from 3.2 to 4.1‰ between the Bh and the Ck horizons (Table 4). This $\Delta_{SOM\text{-}CO_2}$ increase is likely due to a drastic change in porosity (from microporosity to macroporosity; Fig. 2). The Δ between the SOM and the soil CO_2 measured in Villiers are in agreement with those observed in the literature (e.g. Cerling and Wang, 1996; Kutsch et al., 2009).

The theoretical diffusive coefficient (ε) of $^{12}CO_2$ is 1.0044 times greater than ε $^{13}CO_2$ (Craig, 1953). This leads to the well-known

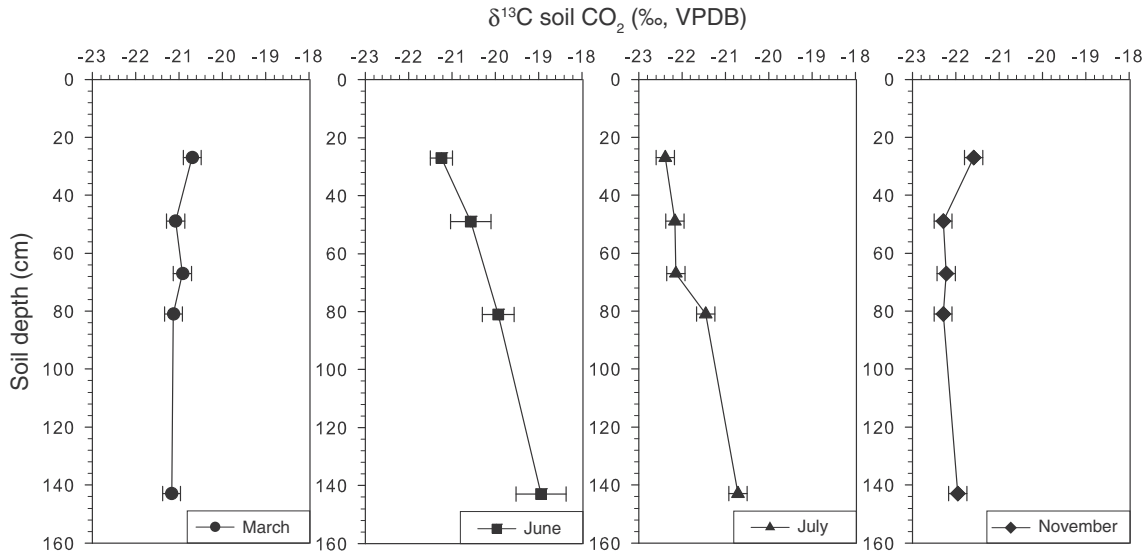

Fig. 5. Examples of C isotopic compositions of soil CO_2 along the profile in function of depth. Vertical distribution of $\delta^{13}C$ values of soil CO_2 for March, June, July, and November 2008.

Table 3
Seasonal variations of the C isotopic composition of CO_2 in the reference soil profile. NA (not available).

Date	Depth (cm)	$\delta^{13}C_{CO_2}$ (‰ VPDB)	Std. dev. (‰ VPDB)	Date	Depth (cm)	$\delta^{13}C_{CO_2}$ (‰ VPDB)	Std. dev. (‰ VPDB)
10.03.08	27	−20.7	0.04	11.06.08	27	−21.2	0.26
10.03.08	49	−21.1	0.13	11.06.08	49	−20.6	0.47
10.03.08	67	−20.9	0.03	11.06.08	67	NA	NA
10.03.08	81	−21.1	0.02	11.06.08	81	−19.9	0.37
10.03.08	143	−21.2	0.10	11.06.08	143	−19.4	0.58
10.03.08	Atm[a]	−11.1	0.03	11.06.08	Atm[a]	−9.8	0.13
17.07.08	27	−22.4	0.05	10.11.08	27	−21.6	0.14
17.07.08	49	−22.2	0.01	10.11.08	49	−22.3	0.16
17.07.08	67	−22.1	0.02	10.11.08	67	−22.2	0.10
17.07.08	81	−21.5	0.06	10.11.08	81	−22.3	0.06
17.07.08	143	−20.7	0.04	10.11.08	143	−22.0	0.06
17.07.08	Atm[a]	−9.6	0.07	10.11.08	Atm[a]	−9.2	0.22

[a] Atmospheric samples were taken at 1.5 m aboveground.

theoretical fractionation (Δ) between the soil CO_2 and its source (SOM), which is equal to +4.4‰ at the soil–atmosphere interface. This influence of the vertical diffusive fractionation towards the atmosphere is observed in the uppermost Ah and Bh horizons until the top of the Bk horizon. Beneath this limit (in the mineral horizon characterized by macroporosity), there is another process that influences the C isotopic composition of the soil CO_2, a lateral diffusive fractionation. This effect can be expressed by a lateral diffusive coefficient ($\varepsilon_{lateral}$) varying with depth and seasons. The soil CO_2 concentration and the temperature variation were used to assess if diffusion occurs in this scree slope soil. The unusual soil CO_2 distribution along the profile (Fig. 3) suggests that strong lateral transfers of gas mass occur in the mineral horizon. The temperature distribution supports a possible convective movement of air masses due to temperature gradients (heat pump effect). The consequence of such a process in a highly macroporous material enhances direct lateral connections with the atmosphere. These types of connections between soil gas and atmosphere have been documented in other studies (e.g. Delaloye et al., 2003). Different topographic, as well as geomorphic, configurations can involve such a process, e.g. break in slopes, anthropogenic artifacts (roads, quarries), etc.

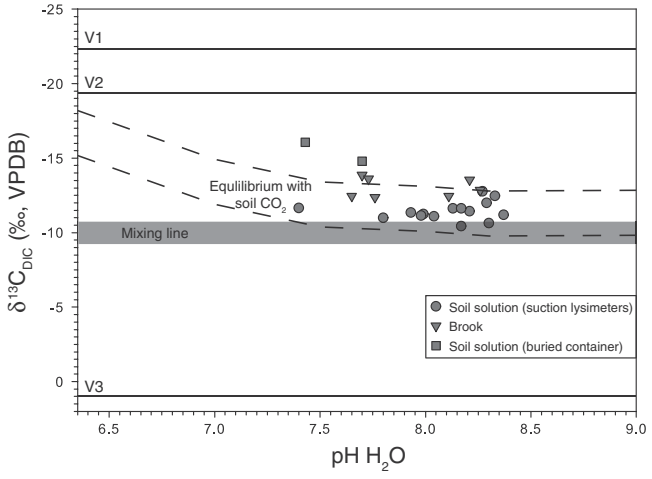

Fig. 6. C isotopic compositions of DIC vs pH values. The dashed line represents the range of the theoretical $\delta^{13}C$ values of DIC in function of the maximum and minimum C isotopic compositions of soil CO_2 measured in Villiers over a one year-period of monitoring. The system is considered as an open system. The values are calculated using the relative contribution of DIC species related to their respective enrichment factors. The solid lines V1, V2, and V3 represent the maximum $\delta^{13}C$ values of soil CO_2, the minimum $\delta^{13}C$ values of the soil CO_2, and the mean $\delta^{13}C$ values of lithogenic carbonate, respectively. The mixing line represents the non-equilibrium mixing between the soil CO_2 and lithogenic carbonate in a closed system, considering the maximum and minimum $\delta^{13}C$ values of the soil CO_2 measured in Villiers.

5.2. The origin of carbon in secondary calcium carbonate precipitations from a scree slope soil (temperate forest)

Carbon transfers between the soil atmosphere and the soil solution strongly depend on pH, temperature at a given depth, and parent rock (Jin et al., 2009). In Ah and Bh horizons, Δ_{CO_2-DIC} ($\Delta_{CO_2-DIC} = \delta^{13}C_{CO_2} - \delta^{13}C_{DIC}$) vary only slightly in function of depth (+10‰ < Δ_{CO_2-DIC} < +10.4‰; Fig. 7 and Table 4). Along this depth interval, average pH values are stable, ranging from 8.2 (at 27 cm deep) to 8.1 (at 49 and 67 cm deep). The Δ_{CO_2-DIC} between the soil $CO_{2(g)}$ and the $HCO_3^-{}_{(aq.)}$ adapted from Clark and Fritz (1997) at 5 °C, is estimated at 10.2‰. Given the mean temperature measured in Villiers, the fractionation values obtained in this scree slope soil are very close to the one obtained using Clark and Fritz (1997) equations. According to the pH measured in the studied soil, the DIC of the soil solution is mainly present as $HCO_3^-{}_{(aq.)}$ in the Ah and Bh horizons. The goodness of fit between the theoretical Δ_{CO_2-DIC} and measured values supports the validation of both sampling and analytical methods.

In the mineral horizons (Bk and Ck) characterized by a coarse skeleton, the Δ_{CO_2-DIC} decreases from 10.3 to 5.8‰ for the deepest sampling depth. This variation in the Δ_{CO_2-DIC} is mainly related to the changes in pH values (7.7 at 100 cm and 7.4 at 157 cm). In this range of pH, the soil solution contains a mixture of $HCO_3^-{}_{(aq.)}$ and $CO_{2(aq.)}$. The relative

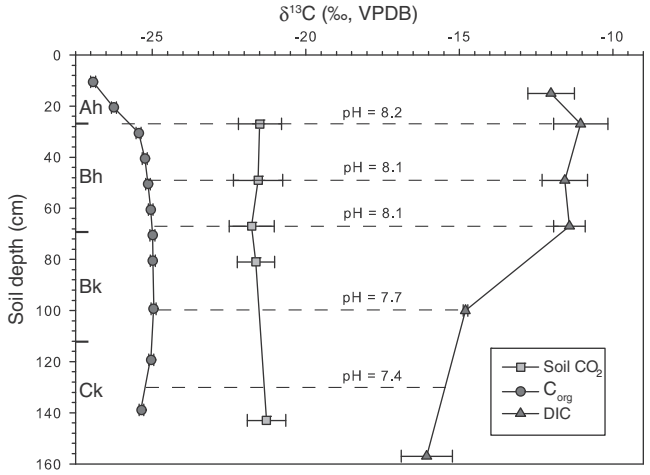

Fig. 7. Plot of the average C isotopic compositions of the various soil compartments (SOM, soil CO_2 and DIC) in function of depth. Fractionation values between SOM and soil CO_2 can be easily followed, as well as the fractionation values between soil CO_2 and DIC. Mean values of pH are given for each corresponding depth. Note that dashed lines are only aids for reading C transfers between the various soil compartments.

Table 4
C isotopic composition of the total organic carbon, mean C isotopic signatures of the soil CO_2 and DIC, pH values of the soil solution, and fractionation values between SOM, CO_2 and DIC. NA (not available).

Depth (cm)	$\delta^{13}C_{org}$ (‰ VPDB)	Mean $\delta^{13}C_{CO2}$ (‰ VPDB)	Std. dev. (‰ VPDB)	Mean $\delta^{13}C_{DIC}$ (‰ VPDB)	Std. dev. (‰ VPDB)	pH	$\Delta^{13}C$ C_{org}–CO_2 (‰ VPDB)	$\Delta^{13}C$ CO_2–DIC (‰ VPDB)
20	−26.2	NA	NA	−12.0	0.8 (n = 3)	NA	NA	NA
30	−25.4	−21.5	0.7 (n = 4)	−11.0	0.9 (n = 4)	8.2	3.9	10.4
50	−25.1	−21.6	0.8 (n = 4)	−11.6	0.7 (n = 8)	8.1	3.6	10.0
70	−25.0	−21.8	0.7 (n = 3)	−11.4	0.5 (n = 7)	8.1	3.2	10.4
100	−25.0	−21.6	0.6 (n = 3)	−14.8	0.1 (n = 4)	7.7	3.3	6.8
140	−25.3	−21.3	0.6 (n = 3)	−16.1	0.8 (n = 3)	7.4	4.1	5.2

contribution of these two DIC species in the soil solution determines the $\delta^{13}C_{DIC}$ values.

The $\delta^{13}C$ values of both soil solution and soil gas indicate that DIC is in equilibrium with soil CO_2 along the entire soil profile (Fig. 4). Moreover, the results are in agreement with the in situ temperature and pH. These results confirm that the main carbon source for DIC is the heterotrophic recycling and oxidation (respiration) of SOM and not the dissolution of lithogenic carbonates (limestone). The DIC would have been more ^{13}C-enriched (higher $\delta^{13}C_{DIC}$ values) if weathering of the parent rock ($\delta^{13}C_{car} = 1.1 \pm 0.1$‰) had a greater influence on the system. Such results are not trivial as the study area is located in a temperate carbonate soil, where the weathering effect could be expected to be much stronger.

Regarding C transfers between the soil solution and pedogenic carbonate (in this case, mainly needle fiber calcite with −8.4 ± 0.1‰ $\delta^{13}C$; see Millière et al., 2011b and Cailleau et al., 2009 for details), $\delta^{13}C$ values of pedogenic carbonate suggest that the C source mainly originates from the DIC species. According to the theoretical model (Clark and Fritz, 1997), it is possible to predict the behavior of the DIC during the progressive evaporation of soil water and the concomitant secondary $CaCO_3$ precipitation. Variation of soil pH would change the concentration ratios of the various DIC species, inducing changes in the C isotopic composition of the pedogenic $CaCO_3$ as it forms. However, the primary C-source of the dissolved inorganic carbon and the NFC and LCC remain unchanged. This point should be cautiously considered if the pH falls far beyond the stability for calcite, which could lead to an enhanced input from the inherited lithogenic carbonate.

5.3. Changes in Rock-Eval HI, OI, and $\delta^{13}C_{SOM}$ during decay of soil organic matter in a temperate climate environment

Four hypotheses have been formulated to explain the ^{13}C enrichment in SOM with increasing depth: (i) a change in the isotopic composition of atmospheric carbon, (ii) changes in the microbial biomass in deeper horizons, (iii) kinetic fractionation during plant respiration, and (iv) preferential decay of labile organic compounds (Boström et al., 2007; Wynn et al., 2006).

The $\delta^{13}C_{SOM}$ values vary between −26.9 and −25.0‰ with depth (Fig. 4). Trends towards higher values with depth suggest a decay of the SOM fraction with a release of isotopically light moieties (e.g., CO_2, short-C-chain lipids). OI values increased with depth from ~183 to ~377 mg CO_2/g C_{org}, and HI values decreased from ~186 to ~84 mg HC/g C_{org}. The opposite trends between the $\delta^{13}C_{SOM}$ and OI and HI values suggest that oxidation of SOM, through oxidative decarboxylation along the soil profile, is most probably the main process triggering the ^{13}C-enrichment (Fig. 4).

In conclusion, the Rock-Eval HI, OI, and $\delta^{13}C$ values bring new insights into SOM degradation during soil genesis. These results support the hypothesis of a preferential decay of given organic components in soils. Nevertheless, these results cannot be generalized to other soils, as different humification pathways may occur in soils with different SOM composition.

5.4. A synthesis of the main carbon pathways in temperate carbonate scree slope soils

The main carbon compartments, as well as the principal pathways implied in the carbon transfers within the ecosystem, are presented in Fig. 8. First of all, carbon moves from the atmosphere to soil organic matter using photosynthesis fixation, litter deposition, and root exudation. The $\delta^{13}C_{SOM}$ values, ranging from −26.9‰ to −25.0‰ VPDB according to depth, are in balance with the local C_3 vegetation. The main aboveground input of SOM is the *F. sylvatica* litter (with relatively light $\delta^{13}C$ values equal to −29.9‰ ± 0.2‰ VPDB). For the belowground contribution, the rhizodeposition and root exudation constitute the second most important SOM input. Once all these inputs are incorporated into the soil, the microflora metabolizes the SOM pool, resulting in combinations of CO_2 and root respiration, leading to the soil CO_2 compartment. At this stage, the soil CO_2 can return to the atmospheric pool by diffusion or continue its evolution inside the soil. The soil gas is in equilibrium with the soil solution and consequently, DIC concentrations are pCO_2-dependent. For the given temperature and according to Henry's law, the soil CO_2 has a high dissolution coefficient in soil water. As a result, the contribution of weathered lithogenically-derived DIC to the soil solution is negligible. A part of the DIC pool is exported through leachates out of the system, and concomitantly, the remaining DIC may contribute to secondary calcium carbonate precipitation in the mineral horizons. Finally, the soil physicochemical conditions play a fundamental role in these scree slope deposits, allowing an enhanced precipitation of secondary carbonate. Indeed, strong infero-fluxes of gas occur inside the mineral horizons (Bk and Ck) and induce changes in the soil pCO_2 between the various soil layers. Precipitation of secondary carbonate is favored in scree slope deposits, where a convective movement of air masses driven by temperature gradients during summer enhances degassing of CO_2 in mineral horizons. This is in line with observations from Breecker et al. (2009), suggesting calcium carbonate forms when soils are warm and very dry.

6. Conclusions and perspectives

The characterization of the soil carbon dynamics is important to better understand the carbon cycle in the various terrestrial environments (Kutsch et al., 2009). The present study shows that, at Villiers, the carbon contained in secondary pedogenic carbonate (NFC and LCC) mainly originates from atmospheric CO_2 (through the continuum photosynthesis fixation–organic matter decay–root respiration–DIC equilibrium–$CaCO_3$ precipitation), although lithogenic carbonate is present in large amounts in these scree slope deposits. As a consequence, the C isotopic composition of the soil solution reveals that the carbon cycle is dominated by the heterotrophic respiration of the soil biomass, even if this soil is developed on a carbonate substrate. In addition, the relationships between the various soil compartments and the atmosphere are highlighted and should be taken into account for a more exhaustive understanding of the carbon cycle in temperate carbonate scree slope soils.

However, some questions are still pending: (i) what amount of atmospheric CO_2 is exported by the soil solution from dissolved inorganic

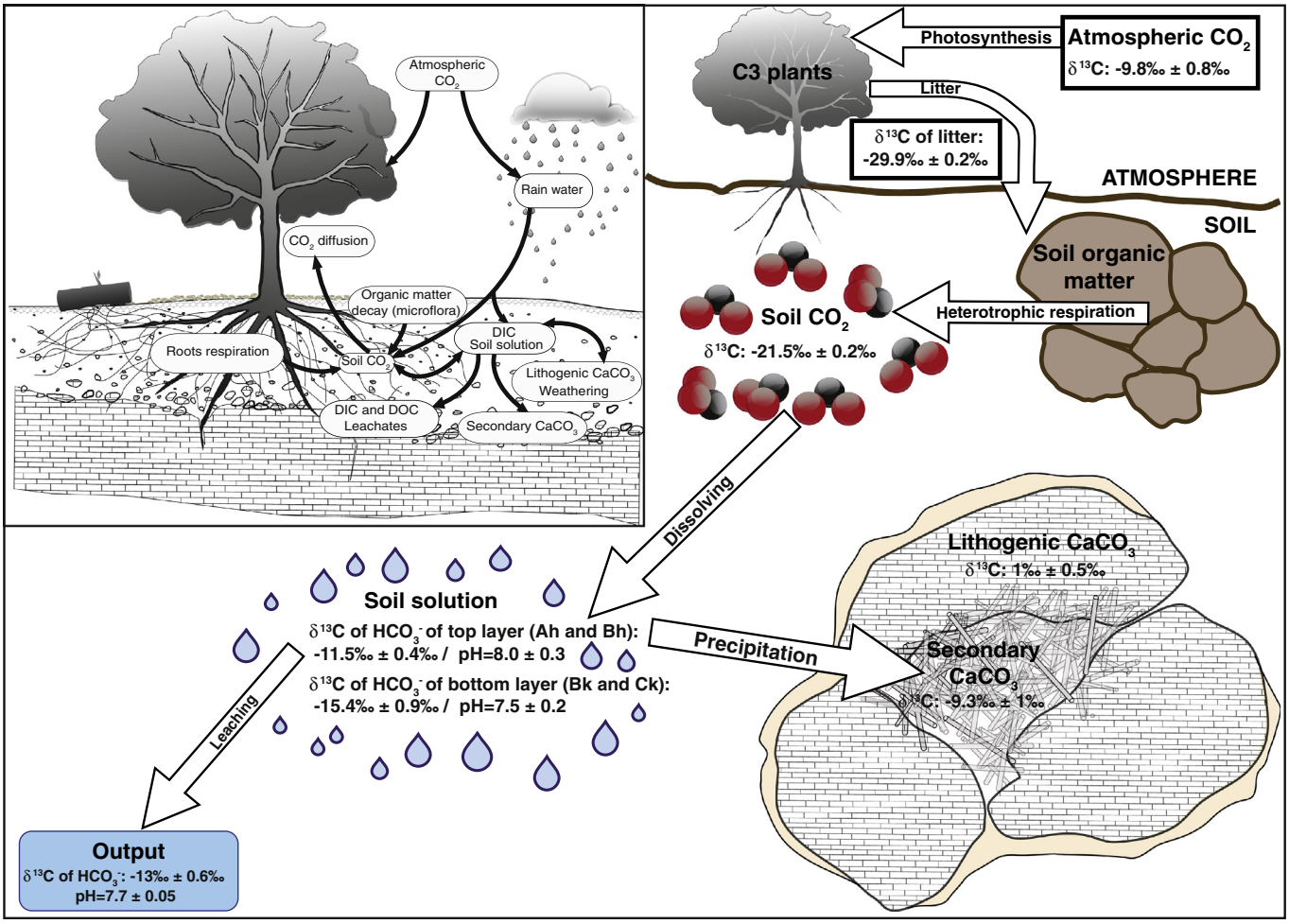

Fig. 8. General pathways of carbon between the various compartments of the Villiers ecosystem. Left-hand corner: sketch representing the main carbon pools and potential processes involved in carbonate soils, based on the common knowledge of ecosystem functioning. Right-hand corner: sketch of the main C pathways occurring between the different soil compartments in a carbonate scree slope soil. The various monitored compartments are presented, as well as the principal processes involved in the carbon transfers within the ecosystem. The white arrows correspond to the processes involved in atmospheric CO_2 transit from the atmosphere to the soil as pedogenic carbonate (NFC and LCC). The mean $\delta^{13}C$ value of the output is −13‰ (n = 7), ranging from −13.9 to −12.4‰ with a standard deviation of 0.6‰. The mean $\delta^{13}C$ value of atmospheric CO_2 is −9.8‰ (n = 4), ranging from −11.1 to −9.2‰ with a standard deviation of 0.8‰. The mean $\delta^{13}C$ value of pedogenic carbonate (NFC and LCC) is −9.3‰ (n = 56), ranging from −10.9 to −7.2‰ with a standard deviation of 1‰ (Millière et al., 2011a,b). The mean $\delta^{13}C$ value of lithogenic carbonate is 1‰ (n = 10), ranging from 0.4 to 1.5‰ with a standard deviation of 0.5‰ (Millière et al., 2011b).

and organic carbon (DIC and DOC) species? (ii) What is the origin of calcium contained in secondary pedogenic calcium carbonate? (iii) And what could be the influence of exogenic Ca-bearing minerals contained in soils of the Swiss Jura Mountains? First of all, as stipulated by Janssens et al. (2003) and Siemens (2003), "there is a gap in the European carbon budget". They hypothesized that missing fluxes may account for this gap. Siemens (2003) estimated from published data that the fluxes of DOC and DIC vary around $11 \pm 8\ g \cdot m^{-2} \cdot yr^{-1}$ and noted that these fluxes may explain this gap. Indeed, the same observation was made at the study site in Villiers. A large amount of carbon can be exported by leachates and these are not taken into account in Net Ecosystem Exchange studies, as they do not investigate soil solution dynamics. Some thorough quantitative studies on soil solution dynamics should be implemented in order to test this point. Secondly, it is clear that Ca must originate from an exogenic source to ensure an effective carbon sink in secondary pedogenic carbonate. In the case of dissolution–reprecipitation of lithogenic limestone, the net balance is null. In the Jura Mountains, large amounts of loess deposits have been described covering extensive areas (Pochon, 1978; Martignier et al., 2013; Martignier and Verrecchia, 2013). The next step is the evaluation of the true potential of Jura soils to act as a carbon sink through an in-depth study coupling quantitative biogeochemistry and mineralogy.

Acknowledgments

This work was supported by the Swiss National Science Foundation, grant nos. FNS 646 205320-109497/1 and FNS 205320–122171 and by the GeoNova project with the financial support of the Swiss University Conference (CUS - PCI 2008). The authors would like to thank two anonymous reviewers who substantially helped to improve the first version of the manuscript as well as Karin Verrecchia for correcting the English grammar.

References

Aravena, R., Schiff, S.L., Trumbore, S.E., Dillon, P.J., Elgood, R., 1992. Evaluating dissolved inorganic carbon cycling in a forested lake watershed using carbon isotopes. Radiocarbon 34, 636–645.

Assayag, N., Rive, K., Ader, M., Jezequel, D., Agrinier, P., 2006. Improved method for isotopic and quantitative analysis of dissolved inorganic carbon in natural water samples. Rapid Commun. Mass Spectrom. 20, 2243–2251.

Bond-Lamberty, B., Thomson, A., 2010. A global database of soil respiration data. Biogeosciences 7, 1915–1926.

Boström, B., Comstedt, D., Ekblad, A., 2007. Isotope fractionation and C-13 enrichment in soil profiles during the decomposition of soil organic matter. Oecologia 153, 89–98.

Breecker, D.O., Sharp, Z.D., McFadden, L.D., 2009. Seasonal bias in the formation and stable isotopic composition of pedogenic carbonate in modern soils from central New Mexico, USA. Geological Society of America Bulletin 121, 630–640.

Burkhard, M., Sommaruga, A., 1998. Evolution of the western Swiss Molasse basin: structural relations with the Alps and the Jura belt. In: Mascle, A., Puigdefàbregas, C., Luterbacher, H.P., Fernàndez, M. (Eds.), Cenozoic foreland Basins of Western Europe. Special Publication 134. The Geological Society London, pp. 279–298.
Cailleau, G., Verrecchia, E.P., Braissant, O., Emmanuel, L., 2009. The biogenic origin of needle fibre calcite. Sedimentology 56, 1858–1875.
Cerling, T.E., 1984. The stable isotopic composition of modern soil carbonate and its relationship to climate. Earth Planet. Sci. Lett. 71, 229–240.
Cerling, T.E., Wang, Y., 1996. Stable carbon and oxygen isotopes in soil CO_2 and soil carbonate: theory, practice, and application to some prairie soils of upper midwestern North America. In: Boutton, T.W., Yamasaki, S. (Eds.), Mass Spectrometry of Soils. Marcel Dekker, Inc., New York, pp. 113–132.
Cerling, T.E., Quade, J., Wang, Y., Bowman, J.R., 1989. Carbon isotopes in soils and paleosols as ecology and palaeoecology indicators. Nature 341, 138–139.
Cerling, T.E., Solomon, D.K., Quade, J., Bowman, J.R., 1991. On the isotopic composition of carbon in soil carbon dioxide. Geochim. Cosmochim. Acta 55, 3403–3405.
Clark, I.D., Fritz, P., 1997. Environmental isotopes in hydrogeology. Lewis Publishers, New York (328 pp.).
Craig, H., 1953. The geochemistry of stable carbon isotopes. Geochim. Cosmochim. Acta 3, 53–92.
Dalla Piazza, R., 1996. Géochimie des altérations dans trois écosystèmes sol-végétation tempérés -Application de l'acquisition des caractéristiques chimiques des solutés. (PhD Thesis no 1483). EPFLausanne.
Delaloye, R., Reynard, E., Lambiel, C., Marescot, C., Monnet, R., 2003. Thermal anomaly in a cold scree slope (Creux du Van, Switzerland). 8th International Permafrost Conference, Zürich, Switzerland, pp. 175–180.
Deutz, P., Montañez, I.P., Monger, H.C., Morrison, J., 2001. Morphology and isotope heterogeneity of Late Quaternary pedogenic carbonates: Implications for paleosol carbonates as paleoenvironmental proxies. Palaeogeogr. Palaeoclimatol. Palaeoecol. 166, 293–317.
Disnar, J.R., Guillet, B., Keravis, D., Di-Giovanni, C., Sebag, D., 2003. Soil organic matter (SOM) characterization by Rock-Eval pyrolysis: scope and limitations. Org. Geochem. 34, 327–343.
Ehleringer, J.R., Buchmann, N., Flanagan, L.B., 2000. Carbon isotope ratios in belowground carbon cycle processes. Ecol. Appl. 10, 412–422.
Espitalié, J., Deroo, G., Marquis, F., 1985a. La pyrolyse Rock-Eval et ses applications; première partie. Rev. Inst. Fr. Pétrol. 40, 563–579.
Espitalié, J., Deroo, G., Marquis, F., 1985b. La pyrolyse Rock-Eval et ses applications; deuxième partie. Rev. Inst. Fr. Pétrol. 40, 755–784.
Fierer, N., Chadwick, O.A., Trumbore, S.E., 2005. Production of CO_2 in soil profiles of a California annual grassland. Ecosystems 8, 412–429.
IUSS Working Group, W.R.B., 2006. World reference base for soil resources 2006. World Soil Resources Reports No. 103, 2nd edition FAO, Rome (145 pp.).
Janssens, I.A., Freibauer, A., Ciais, P., Smith, P., Nabuurs, G.-J., Folberth, G., Schlamadinger, B., Hutjes, R.W.A., Ceulemans, R., Schulze, E.-D., Valentini, R., Dolman, A.J., 2003. Europe's terrestrial biosphere absorbs 7 to 12% of European anthropogenic CO_2 emissions. Science 300, 1538–1542.
Jin, L.X., Ogrinc, N., Hamilton, S.K., Szramek, K., Kanduc, T., Walter, L.M., 2009. Inorganic carbon isotope systematics in soil profiles undergoing silicate and carbonate weathering (Southern Michigan, USA). Chem. Geol. 264, 139–153.
Kutsch, W.L., Bahn, M., Heinemeyer, A., 2009. Soil carbon dynamics — an integrated methodology. Cambridge University Press (286 pp.).
Lafargue, E., Marquis, F., Pillot, D., 1998. Rock-Eval 6 applications in hydrocarbon exploration, production and soil contamination studies. Rev. Inst. Fr. Pétrol. 53, 421–437.
Lal, R., 2009. Sequestering carbon in soils of arid ecosystems. Land Degrad. Dev. 20, 441–454.
Le Quéré, C., Rödenbeck, C., Buitenhuis, E.T., Conway, T.J., Langenfelds, R., Gomez, A., Labuschagne, C., Michel Ramonet, M., Nakazawa, T., Metzl, N., Gillett, N., Heimann, M., 2007. Saturation of the southern ocean CO_2 sink due to recent climate change. Science 316, 1735–1738.
Liu, W., Moriizumi, J., Yamazawa, H., Lida, T., 2006. Depth profiles of radiocarbon and carbon isotopic compositions of organic matter and CO_2 in a forest soil. J. Environ. Radioact. 90, 210–223.
Liu, Z., Dreybrodt, W., Wang, H., 2010. A new direction in effective accounting for the atmospheric CO_2 budget: considering the combined action of carbonate dissolution, the global water cycle and photosynthetic uptake of DIC by aquatic organisms. Earth Sci. Rev. 99, 162–172.
Manning, D.A.C., 2008. Biological enhancement of soil carbonate precipitation passive removal of atmospheric CO_2. Mineral. Mag. 72, 639–649.
Martignier, L., Verrecchia, E.P., 2013. Weathering processes in superficial deposits (regolith) and their influence on pedogenesis: a case study in the Swiss Jura Mountains. Geomorphology 189, 26–40.
Martignier, L., Adatte, T., Verrecchia, E.P., 2013. Bedrock versus superficial deposits in the Swiss Jura Mountains: what is the legitimate soil parent material? Earth Process. Landf. 38, 331–345.
MétéoSuisse, 2008. Office fédéral de Météorologie et de Climatologie, Swiss Normal Climate years 1961–1990. www.meteosuisse.admin.ch/web/fr/climat/climat_en_suisse/climatogrammes_de_stations_meteorologique_suisses.html.
Millière, L., Hasinger, O., Bindschedler, S., Cailleau, G., Spangenberg, J.E., Verrecchia, E.P., 2011a. Stable carbon and oxygen isotope signature of pedogenic needle fibre calcite: further insight on its origin. Geoderma 161, 74–87.
Millière, L., Spangenberg, J.E., Bindschedler, S., Cailleau, G., Verrecchia, E.P., 2011b. Reliability of stable carbon and oxygen isotope compositions of pedogenic needle fibre calcite as environmental indicators: examples from Western Europe. Isot. Environ. Health Stud. 47, 1–18.
Nordt, L.C., Wilding, L.P., Hallmark, C.T., Jacob, J.S., 1996. Stable carbon isotope composition of pedogenic carbonates and their use in studying pedogenesis. In: Boutton, T.W., Yamasaki, S. (Eds.), Mass Spectrometry of Soils. Marcel Dekker, Inc., New York, pp. 133–154.
Park, R., Epstein, S., 1960. Carbon isotope fractionation during photosynthesis. Geochim. Cosmochim. Acta 21, 110–126.
Parkhurst, D.L., Appelo, C.A.J., 1999. User's guide to PHREEQC (Version 2) — a computer program for speciation, batch reaction, one-dimensional transport, and inverse geochemical calculations. 99–4259. U.S. Geological Survey, Denver.
Pochon, M., 1978. Origine et évolution des sols du Haut Jura Suisse. Mémoires de la Société Helvétique des Sciences Naturelles Band/Vol. XC (190 pp.).
Renforth, P., Manning, D.A.C., Lopez-Capel, E., 2009. Carbonate precipitation in artificial soils as a sink for atmospheric carbon dioxide. Appl. Geochem. 24, 1757–1764.
Retallack, G.J., 2007. Soils and global change in the carbon cycle over geological time. In: Holland, H.D., Turekian, K.K. (Eds.), Treatise on geochemistry 5. Pergamon Press, Oxford, pp. 581–605.
Ryskov, Y.G., Demkin, V.A., Oleynik, S.A., Ryskova, E.A., 2008. Dynamics of pedogenic carbonate for the last 5000 years and its role as a buffer reservoir for atmospheric carbon dioxide in soils of Russia. Glob. Planet. Chang. 61, 63–69.
Sanderman, J., 2012. Can management induced changes in the carbonate system drive soil carbon sequestration? A review with particular focus on Australia. Agric. Ecosyst. Environ. 155, 70–77.
Sebag, D., Disnar, J.R., Guillet, B., Di Giovanni, C., Verrecchia, E.P., Durand, A., 2006. Monitoring organic matter dynamics in soil profiles by Rock-Eval pyrolysis: bulk characterization and quantification of degradation. Eur. J. Soil Sci. 57, 344–355.
Siemens, J., 2003. The European carbon budget: a gap. Science 302, 1681.
Szramek, K., McIntosh, J.C., Williams, E.L., Kanduc, T., Ogrinc, N., Walter, L.M., 2007. Relative weathering intensity of calcite vs. dolomite in carbonate-bearing temperate zone watersheds: carbonate geochemistry and fluxes from catchments within the St. Lawrence and Danube River Basin. Geochem. Geophys. Geosyst. 8, Q04002.
Urey, H.C., 1947. The thermodynamic properties of isotopic substances. J. Chem. Soc. 562–581.
Wynn, J.G., Harden, J.W., Fries, T.L., 2006. Stable carbon isotope depth profiles and soil organic carbon dynamics in the lower Mississippi Basin. Geoderma 131, 89–109.